Environ. Sci. Technol. **2003**, *37,* 915−922

Lead Sorption onto Ferrihydrite. 2. Surface Complexation Modeling

JAMES A. DYER,*,†,‡ PARAS TRIVEDI,† NOEL C. SCRIVNER,‡ AND DONALD L. SPARKS†

Department of Plant and Soil Sciences, University of Delaware, Newark, Delaware 19717, and DuPont Engineering Technology, Brandywine Building, Wilmington, Delaware 19898

Few studies have combined molecular- and macroscopic-scale investigations with surface complexation model (SCM) development to predict trace metal speciation and partitioning in aqueous systems over a broad range of conditions. In this work, an extensive collection of new macroscopic and spectroscopic data was used to assess the ability of the modified triple-layer model (TLM) to predict single-solute lead(II) [Pb(II)] sorption onto 2-line ferrihydrite in $NaNO_3$ solutions as a function of pH, ionic strength, and concentration. Regression of constant-pH isotherm data together with potentiometric titration and pH edge data was a much more rigorous test of the TLM than fitting pH edge data alone. When combined with spectroscopic data, the choices of feasible surface species/site types were limited to a few. In agreement with the spectroscopic data, very good fits of the isotherm data were obtained with a two-species, one-site model using the bidentate-mononuclear/monodentate-mononuclear species pairs, $(\equiv FeO)_2Pb/\equiv FeOHPb^{2+}$ and $(\equiv FeO)_2Pb/\equiv FeOPb^{+}-NO_3^{-}$. Regressing edge data in the absence of isotherm and spectroscopic data resulted in a fair number of surface-species/site-type combinations that provided acceptable fits of the edge data but unacceptable fits of the isotherm data. Surprisingly, best-fit equilibrium "constants" for the Pb(II) surface complexes required adjustment outside the pH range of 4.5−5.5 in order to fit the isotherm data. In addition, a surface activity term was needed to reduce the ionic strength dependence of sorption for the species pair, $(\equiv FeO)_2Pb/\equiv FeOHPb^{2+}$. In light of this, the ability of existing SCMs to predict Pb(II) sorption onto 2-line ferrihydrite over a wide range of conditions seems questionable. While many advances have been made over the past decade, much work still needs to be done in fine-tuning the thermodynamic framework and databases for the SCMs.

Introduction

Numerous commercial and public domain geochemical codes exist for predicting trace metal speciation in aqueous systems; however, the existing surface complexation models (SCMs) in these codes often prove inadequate for simulating multisolute sorption reactions in complex industrial systems. One contributing factor is that published thermodynamic parameters for the surface complexes are often based on regressions of a handful of pH sorption edges covering a narrow range of conditions, done without the aid of state-of-the-art spectroscopic techniques to confirm surface speciation.

Extensive studies of metal cation and anion sorption onto amorphous iron (hydr)oxides have been conducted over the years. Dzombak and Morel (*1*) critically reviewed pre-1990 single-solute sorption data for hydrous ferric oxide (HFO); these data were regressed to obtain best-fit intrinsic equilibrium constants (K^{int}) for the Generalized Two-Layer Model (GTLM). Interestingly, only 17% of 184 cation/anion data sets were equilibrium isotherms. This suggests that these equilibrium constants will have limited applicability if the pH edges used to determine them did not cover a broad enough range of conditions. Constant-pH equilibrium isotherms, on the other hand, often cover 5−8 orders of magnitude in metal concentration. If generated at multiple pH values, regression of constant-pH isotherm data along with pH sorption edge data is a much more rigorous test of the SCM.

Despite the fact that lead(II) [Pb(II)] is a common constituent found in contaminated soils, sediments, and some groundwater streams, previous studies of single-solute Pb(II) sorption onto HFO/ferrihydrite are somewhat limited (*1*, *2*). All studies report pH edge data except for Scheinost et al. (*2*), which contains kinetic data for Pb(II) sorption onto 2-line ferrihydrite at pH 5, and Benjamin (*3*), which provides the only published Pb(II) sorption isotherm for HFO (pH 4.5) prior to this work. Interestingly, Dzombak and Morel (*1*) regressed only low concentration edge data to obtain a best-fit K^{int} for Pb(II) sorption onto type 1, high-affinity sites; K^{int} for type 2, low-affinity sites in the GTLM was estimated based on linear free energy relationships.

Before the advent of in situ spectroscopic and microscopic techniques, researchers were limited in their ability to probe the surface of mineral oxides to determine surface speciation. As a result, assumptions about surface speciation in early applications of SCMs were largely based on macroscopic observations, such as the shift (or lack thereof) in pH sorption edges with ionic strength (*4*−*8*). Dzombak and Morel's work (*1*) represented one of the first attempts to use a single SCM to regress a wide cross section of metal sorption data for a single sorbent. Even in recent years, however, pH edge data alone are still being used to obtain best-fit model parameters for SCMs (*9*−*12*). Since 1995, some studies have evaluated the applicability of SCMs over a wider range of concentration, pH, and ionic strength conditions (*13*−*15*). For example, Katz and Hayes (*13*, *14*) proposed a surface continuum model for simulating cobalt(II) sorption onto ∝-Al_2O_3 from 0.05 to 100% surface coverage. Robertson and Leckie (*15*) evaluated the ability of three different SCMs to predict copper (Cu) sorption onto goethite over 3 and 6 orders of magnitude in Cu surface coverage and solution concentration, respectively, at three different pH values. None of these studies, however, benefited from parallel spectroscopic investigations. A handful of studies have combined spectroscopic and macroscopic analyses with surface complexation modeling to simulate trace metal sorption data (*16*−*18*); however, none were found for Pb(II) sorption onto HFO/ferrihydrite.

Application of a Law of Mass Action (LMA)-based SCM requires the definition of many parameters including site densities and surface areas for the sorbents; equilibrium constants for protonation, deprotonation, metal sorption, and background electrolyte sorption reactions; and, in some

* Corresponding author e-mail: james.a.dyer@usa.dupont.com; phone: (302)774-2237; fax: (302)774-1347.
† University of Delaware.
‡ DuPont Engineering Technology.

10.1021/es025794r CCC: $25.00
Published on Web 02/05/2003

cases, capacitance values. This is in addition to making assumptions about the number and types of sorption sites and surface species (*19*). In recent years, Sverjensky and coworkers have developed techniques for estimating the values of a number of LMA-based SCM parameters on the basis of the physical and chemical properties of the solutes and sorbents themselves (*20*−*23*); however, these predictive techniques are currently limited to crystalline sorbents. For an amorphous sorbent like ferrihydrite, regression of macroscopic data is still necessary. In an attempt to address potential limitations inherent in LMA-based SCMs (most notably, the mass balance constraints on surface sites), Kulik has developed a multisite Gibbs energy minimization (GEM) approach for surface complexation modeling (*24*, *25*). Two important aspects of this work are the rigorous definition of standard and reference states for surface species and sites and the use of a surface activity term to suppress the concentration of a surface complex as it nears a defined maximum site density.

An in-depth literature review highlighted the scarcity of studies where molecular- and macroscopic-scale data have been coupled with surface complexation modeling to predict metal-cation sorption over a wide range of conditions. In the first paper in this series, Trivedi et al. (*26*) presented extensive single-solute macroscopic and spectroscopic data for Pb(II) sorption onto 2-line ferrihydrite. In this paper, we highlight the importance of integrating spectroscopic data on surface speciation with macroscopic isotherm and pH sorption edge data covering a wide range of conditions when calibrating a SCM. In addition, we test the ability of the modified triple-layer model to predict single-solute Pb(II) sorption onto 2-line ferrihydrite over a broad range of conditions using a single set of surface complexation modeling parameters.

Methods

Potentiometric Titration and Pb(II) Sorption Data. Modeling studies were based on macroscopic and spectroscopic data for single-solute Pb(II) sorption onto 2-line ferrihydrite (N_2 atmosphere, room temperature, and 4-h equilibration time) that are reported and discussed in ref *26*. This includes the ferrihydrite preparation method as well as potentiometric titration data for ferrihydrite in 0.001, 0.01, and 0.1 M $NaNO_3$ solutions (N_2 atmosphere and room temperature). Raw tabulated titration and Pb(II) sorption data can be found in ref *27*. Titration data at each ionic strength were tabulated as excess acid (q, equiv/L) versus pH:

$$q\ (\text{equiv/L}) = C_A - C_B - [H^+] + [OH^-] \qquad (1)$$

where C_A and C_B are the total quantity of mineral acid and base, respectively, added at each titration point (in equiv/L). The measured pH values at each ionic strength were used to determine molal concentrations for $[H^+]$ and $[OH^-]$ by taking into account activity coefficients for H^+ and OH^- and H_2O activity. The titration curves were then shifted slightly downward along the y-axis so that the common intersection point was at $q = 0.0$. All constant-pH isotherm and pH edge data points were individually equilibrated in their own sample vials.

Geochemical Modeling Software. The OLI Software (OLI Systems, Inc., Morris Plains, NJ) is a commercial simulation package that models aqueous electrolyte equilibria including chemical speciation and redox reactions; equilibria between aqueous, vapor, organic liquid, and multiple solid phases; biochemical and inorganic reaction kinetics; and ion exchange, adsorption, and coprecipitation phenomena. The system is built around the OLI Engine, which is the foundation for the Environmental Simulation Program (ESP), Corrosion Simulation Program (CSP), and ProChem. ProChem was used in this study because it models single-stage equilibria at both steady and unsteady states (*28*).

At the heart of the OLI Engine are the databank, the thermodynamic framework, and the equation solvers (*29*). The OLI databank contains the thermodynamic and physical properties of over 8300 inorganic and organic species. The thermodynamic variables (Gibbs free energy, enthalpy, entropy, and heat capacity) in the databank are from six main sources—Glushko et al. (*30*), Wagman et al. (*31*), Gurvich et al. (*32*), Chase et al. (*33*), Daubert and Danner (*34*), and Oelkers et al. (*35*). Each of these sources is an extensive, carefully evaluated, and well-referenced compilation of thermodynamic data. The state-of-the-art thermodynamic framework uses generalized correlations based upon regressed experimental data in the databank to predict the required thermodynamic and physical properties for the chemical system of interest (i.e., infinite dilution, standard-state values for Gibbs free energy, enthalpy, entropy, heat capacity, and volume, liquid-phase activity coefficients for systems at finite concentrations, etc.). The theoretical basis for the thermodynamic framework is explained elsewhere (*36*, *37*). Shock and Helgeson (*38*) describe the semitheoretical basis for temperature and pressure extrapolation of standard-state properties along with procedures for estimating missing parameters. The aqueous activity coefficient model is an extension of the work of Bromley and Meissner (i.e., the Bromley−Zemaitis framework) and is given in Supporting Information (*37*, *39*). Details on the equation solvers used to solve the nonlinear equilibrium, electroneutrality, and mass balance equations can be found in ref *29*. Permissible operating ranges for the software can be found in ref *40*. The OLI equilibrium reactions and associated equilibrium constants used in this work are given in Table S1 in the Supporting Information.

Surface Complexation Models. Four different surface complexation models are available in the OLI Software—the nonelectrostatic model (NEM), the constant capacitance model (CCM), the GTLM, and the modified triple-layer model (TLM). In this research, the NEM, GTLM, and TLM were all considered, although the TLM ultimately proved to be the preferred SCM as discussed below. The thermodynamic frameworks for the NEM, GTLM, and modified TLM are described in Hayes and Katz (*41*), Dzombak and Morel (*1*), and Sahai and Sverjensky (*42*), respectively.

Modeling Protocol. Hayes and Katz (*41*) served as a basis for the modeling protocol used in this study. First, the OLI Software's nonlinear regression routine was used to determine a valid set(s) of metal hydroxide surface parameters for the SCM of interest using potentiometric titration data for 2-line ferrihydrite at three different ionic strengths as reported in ref *26*. For the GTLM, this was done for a range of site density (N_s) values at a fixed specific surface area (A_s), giving K_{a1}^{int} and K_{a2}^{int} (the surface acidity constants) as a function of N_s. For the modified TLM, Hayes and Katz (*41*) showed that various combinations of N_s, C_1, and ΔpK_a will provide adequate fits of potentiometric titration data for mineral oxides. For this reason, a three-factor, face-centered cube (FCC), response-surface experimental design was used to determine the values of N_s, C_1, and ΔpK_a that provide the best fit of the titration data (A_s and C_2 were held constant in the model). The experimental design was generated and analyzed using the MINITAB Statistical Software (Minitab Inc., State College, PA). Ranges of values considered for N_s, C_1, and ΔpK_a in the experimental design were 0.2−0.9 mol of sites/mol of Fe, 0.6−1.4 faraday/m^2, and 3.0−6.0, respectively. The criteria for judging the quality of fit were the value of R_{avg}, obtained from the OLI code's nonlinear regression program, and visual inspection of a plot of the model titration curves with the experimental data. A Marquardt nonlinear optimization algorithm was used throughout this work; the

objective function minimized was the ratio (R_i) of the calculated to experimental values (or vice versa, such that R_i is always ≥1.0). R_i values were equally weighted, with a perfect fit being defined as $R_i = 1.0$. OLI has found that this objective function is more robust than least-squares minimization when regressing data values that range over many orders of magnitude, such as in constant-pH isotherms where Pb(II) solution concentrations will vary over 5−7 orders of magnitude. R_{avg} represents the arithmetic average of all R_i values for the regressed experimental data set.

Next, spectroscopic results and the impact of ionic strength on Pb(II) sorption were used to guide the selection of the Pb(II) surface complexation reactions at low to moderate surface coverage. Hayes and Katz (*41*) note that past X-ray absorption fine structure spectroscopy (XAFS) studies have suggested that mononuclear species predominate at low to moderate surface coverage (0.1−10%) for strongly sorbing metals and at all coverages for weakly sorbing metals. Ionic strength dependence has also been used historically to infer the presence of inner-sphere versus outer-sphere surface complexes (*43*). In this study, pH edges generated at three different ionic strengths were used to assess the ionic strength dependence of Pb(II) sorption. Spectroscopic results are summarized in ref *26*.

Spectroscopic results and the shape of the constant-pH equilibrium isotherms were used to determine the need for multinuclear surface complexation reactions at higher surface coverage (i.e., surface polymers and/or surface precipitates). The constant-pH isotherms were also used to determine a reasonable starting point for N_s and to assess the possibility of site heterogeneity (i.e., the need for more than one site type). Robertson and Leckie (*44*) found that site heterogeneity is likely if the slope of a constant-pH isotherm curve is less than 1.0 at low surface coverage.

On the basis of the above analyses of the macroscopic and spectroscopic data, an appropriate set of oxide surface parameters (N_s, C_1, C_2, ΔpK_a, and A_s) and Pb(II) surface complex species were assumed for the SCM of interest. These surface parameters/species were used to regress the constant-pH isotherm data to obtain a set of best-fit equilibrium constants for single-solute Pb(II) sorption. The best-fit K values were then used to assess how the model predicted the pH edge data at multiple ionic strengths and initial Pb(II) concentrations. Various combinations of viable Pb(II) surface complexes were considered to evaluate the sensitivity of the model fits to the speciation assumptions. The minimum numbers of site types and species that provided the best fit of the isotherm and pH edge data were considered the optimum. Again, R_{avg} values for both x[total Pb(aq)] and y[mol of Pb/mol of Fe] data from the nonlinear regression program together with visual inspection of graphical output were used to judge the quality of the fits. This step was an iterative process whereby the oxide surface parameters were adjusted if N_s was altered.

Results and Discussion

Potentiometric Titration Data. The point of zero net proton charge (pH_{PZNPC}) for 2-line ferrihydrite was determined to be 7.91, which falls within the range of point of zero charge values reported by others (*1*). Figure S1a,b in the Supporting Information and Figure 1 present best fits of the potentiometric titration data for the NEM, GTLM, and TLM, respectively. Corresponding model parameters are given in Table 1. In all cases, A_s was fixed at 600 m^2/g. The NEM fit provides no functionality with ionic strength, and it significantly overpredicts surface charge as pH moves away from the pH_{PZNPC}. The GTLM was better than the NEM and TLM at capturing the sharp curvature in the titration data at the pH extremes; however, it was inferior to the TLM in predicting the more linear surface-charging behavior over the pH range

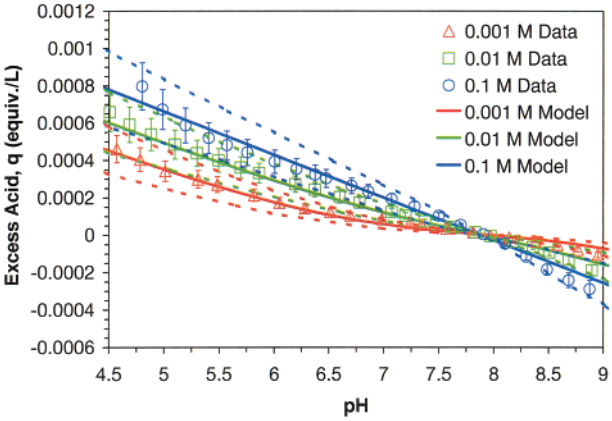

FIGURE 1. Best fit of potentiometric titration data for 2-line ferrihydrite using the modified triple-layer model (TLM). Error bars/bands shown for experimental data and model predictions are ± 2σ. Experimental conditions: 1 g of ferrihydrite/L; 0.001, 0.01, and 0.1 M $NaNO_3$ electrolyte solutions; room temperature; N_2 glovebox; 1-L reactor; 2-min equilibration time at each pH point; 0.1 M NaOH used to raise initial pH to ~10; 0.1 M HNO_3 used to titrate mixture downward to ~pH 4.

of 5−9. Regardless of the number of site types and N_s, the general shape of the GTLM-predicted titration curves did not change substantially.

The modified TLM produced titration curves (Figure 1) that were more linear over a wider pH range, especially as ionic strength increased. Unlike the NEM and GTLM, outer-sphere surface complexes involving the background electrolyte ions are included in the TLM; these complexes dominate surface charge, producing less curvature in the titration curves. The optimum fit shown in Figure 1 along with the associated model parameters in Table 1 were obtained with the help of the three-factor, FCC, response−surface experimental design. The quality of the fits based on R_{avg} was highly sensitive to the value of C_1. On the other hand, the impacts of ΔpK_a and N_s on R_{avg} were moderate and small, respectively. In all cases, the TLM could not reproduce the sharp increase (decrease) in proton surface charge at pH <4.5 (>9) (see Figure 1 in ref *26*). In general, the quality of the TLM fit deteriorated at the pH extremes and as ionic strength increased. For this reason, the model fit of the titration data was optimized over the pH range of 4.5−9.0.

To validate the quality and consistency of the data, ferrihydrite titrations in 0.01 and 0.1 M $NaNO_3$ solutions were repeated two more times each in separate runs as discussed in ref *26*. In all cases, these new titrations occurred 1 year after the original titrations used for the model regressions and used a different batch of ferrihydrite. The additional titrations in 0.01 M $NaNO_3$ solution were conducted over the pH range of 4−10 to examine the effects of a longer equilibration time (15 vs 2 min in original titrations) and a higher solids concentration (10 vs 1 g/L in original titrations). The impact of equilibration time alone was small at 1 g of ferrihydrite/L, suggesting that kinetics was not a significant factor. The combination of a higher solids concentration and longer equilibration time, on the other hand, shifted the 0.01 M $NaNO_3$ titration curve to a lower surface charge and provided some dampening of the sharp curvature at the pH extremes. At this high solids concentration, however, mass transfer limitations were likely. Regardless, the new data did not substantially improve the ability of the TLM to fit the titration data over the entire pH range of 4−10. The 0.1 M $NaNO_3$ titrations were repeated over a narrower pH range (pH 5−9 vs pH 4−10) than the original titration and were conducted from both low-to-high and high-to-low pH. Figure S2 (Supporting Information) shows excellent agreement

TABLE 1. Model Parameters for the NEM, GTLM, and TLM Based on Regression of Potentiometric Titration Data for 2-Line Ferrihydrite at Room Temperature in N_2 Atmosphere

model	N_s (mol/mol)	C_1 (faraday/m^2)	C_2 (faraday/m^2)	log K^{int}_{a1} [a]	log K^{int}_{a2} [b]	log K^{int}_{NO3-} [c]	log K^{int}_{Na+} [d]	R_{avg}
NEM	0.8	na[e]	na	−4.43	−11.52	na	na	6.0
GTLM	0.8	na	na	−6.49	−8.89	na	na	1.6
TLM	0.8	0.725	0.2	−5.41	−10.41	−7.59	8.14	1.2

[a] $\equiv FeOH_2^+ = \equiv FeOH + H^+$, where $K^{int}_{a1} = a_{H+}[\equiv FeOH] \exp(-F\Psi_o/RT)/[\equiv FeOH_2^+]$. [b] $\equiv FeOH = \equiv FeO^- + H^+$, where $K^{int}_{a2} = a_{H+}[\equiv FeO^-] \exp(-F\Psi_o/RT)/[\equiv FeOH]$. [c] $\equiv FeOH_2^+ - NO_3^- = \equiv FeOH + H^+ + NO_3^-$, where $K^{int}_{NO3-} = a_{H+}a_{NO3-}[\equiv FeOH] \exp(F(\Psi_\beta - \Psi_o)/RT)/[\equiv FeOH_2^+ - NO_3^-]$. [d] $\equiv FeO^- - Na^+ + H^+ = \equiv FeOH + Na^+$, where $K^{int}_{Na+} = a_{Na+}[\equiv FeOH] \exp(F(\Psi_o - \Psi_\beta)/RT)/a_{H+}[\equiv FeO^- - Na^+]$. [e] na, not applicable.

between the triplicate 0.1 M $NaNO_3$ runs, indicating that the ferrihydrite preparation and experimental titration methods are reproducible. The results were also similar regardless of the initial conditions. On the basis of the triplicate 0.1 M $NaNO_3$ data, the average coefficient of variation (1σ) for the ~100 titration steps between pH 5 and pH 9 was ~8%. Error bars corresponding to $\pm 2\sigma$ are shown in Figure 1. In addition, independent solubility measurements for 2-line ferrihydrite in 0.01 M $NaNO_3$ solutions over the pH range of 3−5 showed that sorbent dissolution could not account for the sharp increase in acid consumption between pH 5 and pH 4. Ferrihydrite solubility was nondetect, 1.7 ppb, and 6.5 ppb at pH 5, 4.5, and 4, respectively. Ongoing investigations are examining the possibility that the sharp change in slope of the titration curves below pH 4.5 and above pH 9 is due to a change in ferrihydrite morphology and, hence, in the surface area available for reaction with acid or base.

While none of the SCMs could predict the shape of the titration curves over the entire pH range (pH 4−10), the TLM provided the best fits of the ferrihydrite titration data over the pH range of environmental significance (pH 4.5−9). There are several important points to keep in mind regarding the quality of the titration data fits. First, while optimizing the model fit of the titration data over different pH ranges (pH 5−8, 4.5−9, and 4−10) resulted in different sets of best-fit oxide surface parameters (i.e., C_1, log K^{int}_{NO3-}, and log K^{int}_{Na+}), these unique sets of parameters gave essentially identical fits of the constant-pH isotherm data (i.e., log K values for the Pb(II) surface complexes). Second, the model predictions are also bounded by a level of uncertainty. Figure 1 displays the 95% prediction intervals for the model titration curves on the basis of the results of a rigorous error propagation analysis using the uncertainty analysis module in the OLI code (*27*). Assumed input/thermodynamic uncertainties (1σ) were C_1 (10%), C_2 (10%), pH (0.03 unit), total ferrihydrite (10%), total H_2O (3%), total $NaNO_3$ (10%), total NaOH (2.5%), total HNO_3 (2.5%), log K^{int}_{a1} (0.125 log unit), log K^{int}_{a2} (0.125 log unit), log K^{int}_{NO3-} (0.125 log unit), and log K^{int}_{Na+} (0.125 log unit). When uncertainties in the data and model are both considered, the experimental data points fall well within the uncertainty bands for the model curves. Third, extensive uncertainty analyses of the Pb(II) isotherm and pH edge model fits in Dyer (*27*) revealed that input uncertainties in log K^{int}_{NO3-} and log K^{int}_{Na+} have little impact on the predicted output uncertainties in Pb(II) sorbed and Pb(II) in solution over the majority of the pH, Pb concentration, and ionic strength space covered by this study. Only in the narrow pH range of 3.5−4.5 at low Pb(II) surface ($<10^{-3}$ mol/mol) and solution (<1 ppm) concentrations did uncertainty in the titration data fit have a significant impact on predicted Pb(II) partitioning. More importantly, this was true only when the 1σ uncertainties in log K^{int}_{NO3-} and log K^{int}_{Na+} were greater than 0.24 log unit (i.e., a 2σ uncertainty >148% in K space). In all other cases, uncertainties in Pb(II) concentrations were not sensitive to the fit of the titration data. On the basis of consideration of R_{avg}, visual inspection of the fits, extensive uncertainty analyses, and results of past TLM modeling efforts with HFO (*4*, *8*, *45*), Figure 1 was defined as the "best fit" to carry forward for the regression of the Pb(II) sorption data.

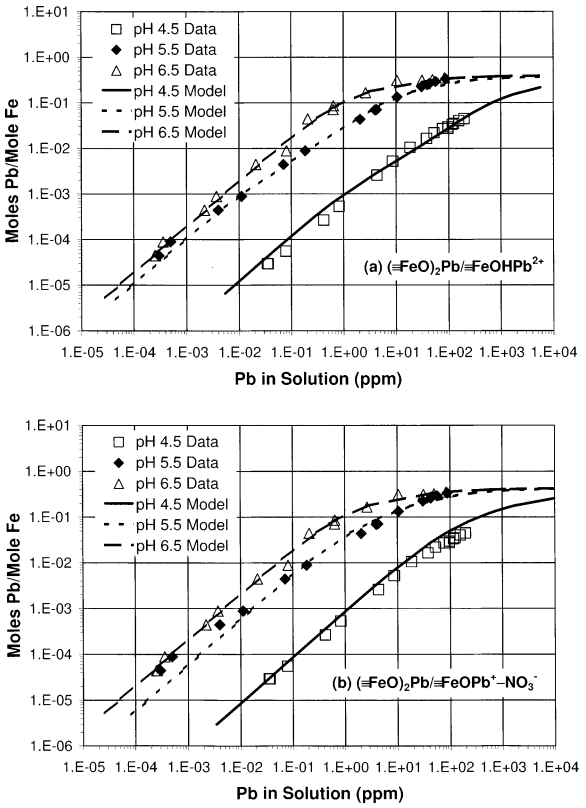

FIGURE 2. Optimized triple-layer model fits of pH 4.5, 5.5, and 6.5 equilibrium isotherm data for single-solute Pb(II) sorption onto 2-line ferrihydrite assuming the species pairs (a) ($\equiv FeO)_2Pb/\equiv FeOHPb^{2+}$ [log $K_{(\equiv FeO)_2Pb}$ = 4.98 (pH 4.5, 5.5) and 6.16 (pH 6.5); log $K_{\equiv FeOHPb^{2+}}$ = −8.76 (pH 4.5, 5.5) and −5.27 (pH 6.5)] and (b) ($\equiv FeO)_2Pb/\equiv FeOPb^+ - NO_3^-$ [log $K_{(\equiv FeO)_2Pb}$ = 5.02 (pH 4.5, 5.5) and 5.95 (pH 6.5); log $K_{\equiv FeOPb^+ - NO_3^-}$ = −2.17 (pH 4.5, 5.5) and −0.18 (pH 6.5)]. Experimental conditions: 0.1 and 1.0 g of ferrihydrite/L in 0.01 M $NaNO_3$ solution; Pb(II) added as $Pb(NO_3)_2$; 4-h equilibration time; room temperature; N_2 glovebox.

Pb(II) Sorption Isotherms and Edges. Analysis of macroscopic and spectroscopic data from ref *26* for Pb(II) sorption onto 2-line ferrihydrite provided several insights to help focus the SCM development. First, pH edge data for 50 μM Pb(II) equilibrated with 1 g of ferrihydrite/L in 0.001, 0.01, and 0.1 M $NaNO_3$ solutions showed only a small ionic strength dependence, indicating the likelihood of inner-sphere surface complexes. Second, the slope of the constant-pH isotherms at low Pb(II) concentrations was approximately 1.0, suggesting that a one-site model would be adequate. Third, the spectroscopic data analysis indicated that a bidentate-mononuclear inner-sphere surface complex dominated at pH 5.5 and pH 6.5, while at pH 4.5 there was evidence for both inner-sphere monodentate-mononuclear and biden-

TABLE 2. TLM Parameters for Single-Solute Pb(II) Sorption onto 2-Line Ferrihydrite (fh) at Room Temperature in N_2 Atmosphere

species pair	pH	log $K_{(\equiv FeO)_2Pb}$ at 1 g fh/L[a,b]	log $K_{\equiv FeOHPb^{2+}}$ or $_{\equiv FeOPb^{+}-NO_3^{-}}$ [c]	R_{avg} (Pb_{aq})[d]	R_{avg} (Γ)[d]
$(\equiv FeO)_2Pb/\equiv FeOHPb^{2+}$	4.5−5.5	4.98	−8.76	1.2	1.1
	6.5	6.16	−5.27	1.2	1.01
	3.0	2.44	−9.57		
	3.5	3.39	−9.51		
	4.0	4.28	−9.26		
	6.0	5.67	−7.50		
$(\equiv FeO)_2Pb/\equiv FeOPb^{+}-NO_3^{-}$	4.5−5.5	5.02	−2.17	1.3	1.1
	6.5	5.95	−0.18	1.2	1.01
	3.0	2.69	−4.02		
	3.5	4.21	−3.45		
	4.0	5.02	−2.85		
	6.0	5.83	−1.53		

[a] $(\equiv FeO)_2Pb + 2H^+ = 2\equiv FeOH + Pb^{2+}$, where $K_{(\equiv FeO)_2Pb} = a_{Pb^{2+}}[\equiv FeOH]^2/a_{H^+}{}^2\gamma_s[(\equiv FeO)_2Pb]$. The γ_s correction applies for $(\equiv FeO)_2Pb/\equiv FeOHPb^{2+}$ only. [b] For bidentate-mononuclear surface complexes, K^{int} is actually a conditional K that depends on sorbent solids concentration, C_s, regardless. This peculiarity arises with multidentate complexes because of the definition of the standard state for surface species in molality rather than mole fraction. It can be shown that $K^{int} = K^{cond}/B$, where $B = N_s$ (sites/m²) × A_s (m²/g) × C_s (g/L)/N_A (6.02 × 10^{23} sites/mol of sites). Hence, $K_2^{cond}/K_1^{cond} = C_{s2}/C_{s1}$ for the bidentate-mononuclear reactions written here as dissociation reactions. The bidentate-mononuclear K values reported in the table are based on 1 g of ferrihydrite/L. [c] $\equiv FeOHPb^{2+} = \equiv FeOH + Pb^{2+}$, where $K_{\equiv FeOHPb^{2+}} = a_{Pb^{2+}}[\equiv FeOH]\exp(-2F\Psi_o/RT)/\gamma_s[\equiv FeOHPb^{2+}]$; and $\equiv FeOPb^{+}-NO_3^{-} + H^+ = \equiv FeOH + Pb^{2+} + NO_3^-$, where $K_{\equiv FeOPb^{+}-NO_3^{-}} = a_{Pb^{2+}}a_{NO_3^-}[\equiv FeOH]\exp(F(\Psi_\beta - \Psi_o)/RT)/a_{H^+}[\equiv FeOPb^{+}-NO_3^{-}]$. [d] R_{avg} reported for regressions of pH 4.5, 5.5, and 6.5 isotherm data only. K values for other pH values are approximate based on regression of a few pH edge points only. The intent is to show how K varies with pH.

tate-mononuclear surface complexes. Fourth, the unequal spacing between the pH 4.5, 5.5, and 6.5 isotherms (changing d[pPb_{aq}]/d[pH] at a constant Pb(II) surface loading) suggested that a unique set of equilibrium constants and/or surface species would not fit all the data. The spectroscopic results, however, gave no indication that a change in surface speciation was the reason for this significant change in spacing between the isotherms. Fifth, the plateau in the pH 5.5 and pH 6.5 isotherm data suggested a maximum Pb(II) surface loading of approximately 0.35−0.40 mol of Pb/mol of Fe.

The constant-pH isotherm data are shown in Figure 2 along with fits obtained using the modified TLM for two different species pairs: $(\equiv FeO)_2Pb$ plus $\equiv FeOHPb^{2+}$ and $(\equiv FeO)_2Pb$ plus $\equiv FeOPb^{+}-NO_3^{-}$. Equilibrium constants, associated equilibrium reactions and mass law expressions, and R_{avg} values for the pH 4.5, 5.5, and 6.5 isotherm fits are summarized in Table 2 for both species pairs. On the basis of a maximum Pb(II) surface loading of 0.35−0.40 mol of Pb/mol of Fe, N_s was optimized at 0.80 mol of sites/mol of Fe. In general, as pH and surface loading increased, the bidentate-mononuclear surface complex became more dominant. The monodentate-mononuclear complexes were more important at lower pH and surface loading. Spectroscopic data were unable to distinguish between the monodentate-mononuclear complexes, $\equiv FeOHPb^{2+}$ and $\equiv FeOPb^{+}-NO_3^{-}$. On the basis of R_{avg} alone, the $(\equiv FeO)_2Pb/\equiv FeOHPb^{2+}$ species pair provided a better fit of the constant-pH isotherms. Regression of the isotherm data using only a one-species model gave inferior fits when compared to a two-species model (Figures S3−S5, Supporting Information). Although not supported by spectroscopic data, the species pair, $\equiv FeOPbOH$ plus $\equiv FeOPb^{+}$, provided essentially the same quality of fit as the bidentate-mononuclear species pairs (Figure S6, Supporting Information). Mathematically, the mass law expression for $\equiv FeOPbOH$ looks much the same as the mass law expression for $(\equiv FeO)_2Pb$. In addition, the two-species, one-site TLM provided superior fits of the isotherm data when compared to the one-species, two-site GTLM (Figures S7 and S8, Supporting Information). The GTLM was evaluated for two cases—using the same site densities and log K values for Pb(II) as proposed by Dzombak and Morel (*1*) (Figure S7) and using modified K values in combination with a much higher type-2 site density of 0.9 mol of sites/mol of Fe (Figure S8).

As shown in Table 2, the same pair of equilibrium constants provided very good fits of both pH 4.5 and pH 5.5

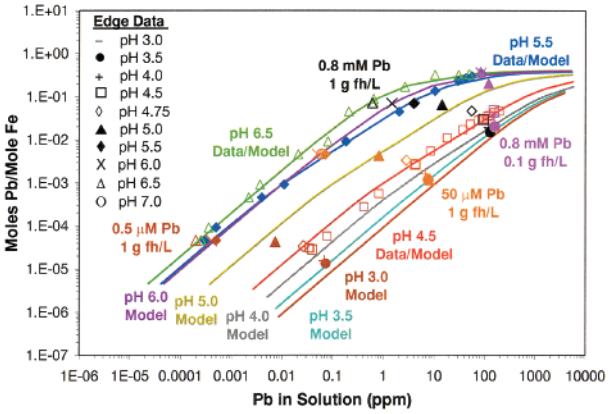

FIGURE 3. Comparison of constant-pH isotherm and pH sorption edge data to modified triple-layer model predictions for single-solute Pb(II) sorption onto 2-line ferrihydrite assuming the species pair $(\equiv FeO)_2Pb/\equiv FeOHPb^{2+}$ [log $K_{(\equiv FeO)_2Pb}$ = 2.44, 3.39, 4.28, 4.98, 5.67, and 6.16 and log $K_{\equiv FeOHPb^{2+}}$ = −9.57, −9.51, −9.26, −8.76, −7.50, and −5.27 at pH 3.0, 3.5, 4.0, 4.5−5.5, 6.0, and 6.5, respectively]. Experimental conditions: 0.1 and 1.0 g of ferrihydrite/L; 0.01 M $NaNO_3$ background electrolyte for isotherms and edges; Pb(II) added as $Pb(NO_3)_2$; 4-h equilibration time; room temperature; N_2 glovebox.

isotherm data over 5 orders of magnitude in Pb(II) concentration. At pH 6.5, however, the values of K^{int} for the Pb(II) surface complexes required adjustment; that is, the binding strength of the surface complexes was reduced. No change in surface speciation or N_s was necessary to fit the pH 6.5 data. For this reason, equilibrium constants for the Pb(II) surface complexes are reported as conditional K values (K_i) rather than as intrinsic K values (K_i^{int}). To explore this further, pH sorption edge data were plotted with isotherm data on the same graph. Figure 3 shows excellent agreement between the pH edge and the isotherm data, indicating that the data are internally consistent. Interestingly, Figure 3 suggests that a reduction in spacing between the constant-pH isotherms should be expected on the basis of the inherent shape of a pH sorption edge. More specifically, d[pPb_{aq}]/d[pH] changes significantly over the course of a pH sorption edge. At low and high values of percent of Pb sorbed, the change in sorbed Pb(II) and, hence, in total [Pb(II)(aq)] is relatively small for a unit change in pH (i.e., d[pPb_{aq}]/d[pH] is small). However, over a narrow pH range, the change in sorbed Pb(II) with pH increases substantially (i.e., d[pPb_{aq}]/

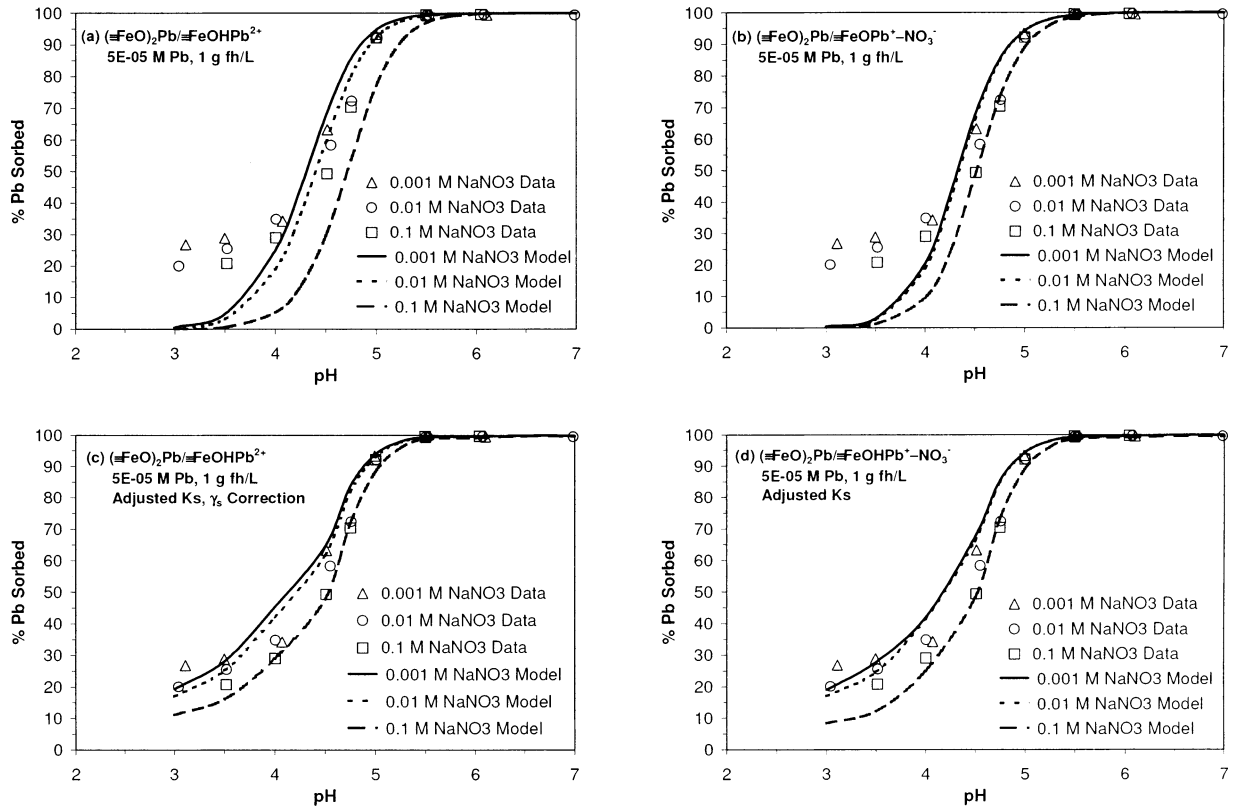

FIGURE 4. Triple-layer model predictions of pH sorption edge data for single-solute Pb(II) sorption onto 2-line ferrihydrite. Fits for (a) $(\equiv FeO)_2Pb/\equiv FeOHPb^{2+}$ using $\gamma_s = 1.0$ and best-fit K values for pH 4.5−5.5 data only [log $K_{(\equiv FeO)_2Pb} = 4.98$ and log $K_{\equiv FeOHPb^{2+}} = -8.76$]; (b) $(\equiv FeO)_2Pb/\equiv FeOPb^{+}-NO_3^{-}$ using $\gamma_s = 1.0$ and best-fit K values for pH 4.5−5.5 data only [log $K_{(\equiv FeO)_2Pb} = 5.02$ and log $K_{\equiv FeOPb^{+}-NO_3^{-}} = -2.17$]; (c) $(\equiv FeO)_2Pb/\equiv FeOHPb^{2+}$ using $\gamma_s = \gamma_{Pb^{2+}}$ correction and pH-adjusted K values from Table 2 [log $K_{(\equiv FeO)_2Pb} = 2.44, 3.39, 4.28, 4.98, 5.67$, and 6.16 and log $K_{\equiv FeOHPb^{2+}} = -9.57, -9.51, -9.26, -8.76, -7.50$, and −5.27 at pH 3.0, 3.5, 4.0, 4.5−5.5, 6.0, and 6.5, respectively]; (d) $(\equiv FeO)_2Pb/\equiv FeOPb^{+}-NO_3^{-}$ using $\gamma_s = 1.0$ and pH-adjusted K values from Table 2 [log $K_{(\equiv FeO)_2Pb} = 2.69, 4.21, 5.02, 5.02, 5.83$, and 5.95 and log $K_{\equiv FeOPb^{+}-NO_3^{-}} = -4.02, -3.45, -2.85, -2.17, -1.53$, and −0.18 at pH 3.0, 3.5, 4.0, 4.5−5.5, 6.0, and 6.5, respectively]. Experimental conditions: 1.0 g of ferrihydrite/L; 0.001−0.1 M $NaNO_3$; 50 μM Pb(II) added as $Pb(NO_3)_2$; 4-h equilibration time; room temperature; N_2 glovebox.

d[pH] is large). For Pb(II), the steep slope of the pH sorption edge occurs over the pH range of 4−5.5 where $d[pPb_{aq}]/d[pH]$ peaks at about 2.0. By pH 6.5, however, the sorption edge has begun to plateau, and $d[pPb_{aq}]/d[pH]$ is 0.5 or less. The constant-pH isotherm curves for pH 3, 3.5, 4, and 6 shown in Figure 3 represent model fits to the pH edge data only for the species pair, $(\equiv FeO)_2Pb$ plus $\equiv FeOHPb^{2+}$. Oxide surface parameters for the TLM (Table 1) and the assumed surface speciation were the same as those used to regress the pH 4.5, 5.5, and 6.5 isotherm data. Conditional equilibrium constants for each pH value are given in Table 2. The pH 5 isotherm curve shown in Figure 3 was predicted using the best-fit log $K_{(\equiv FeO)_2Pb}$ and log $K_{\equiv FeOHPb^{2+}}$ values reported for pH 4.5−5.5 in Table 2. Although not shown, results for the $(\equiv FeO)_2Pb/\equiv FeOPb^{+}-NO_3^{-}$ species pair are very similar; conditional K values as a function of pH are reported in Table 2 as well.

Figure 4 compares TLM predictions to pH edge data reported in ref *26* for 50 μM Pb(II) in equilibrium with 1 g of ferrihydrite/L in 0.001, 0.01, and 0.1 M $NaNO_3$ solutions. Figure 4a displays model predictions for the $(\equiv FeO)_2Pb/\equiv FeOHPb^{2+}$ species pair using (i) best-fit equilibrium constants for the pH 4.5−5.5 data only and (ii) aqueous activity coefficient corrections for bulk solution ions only, i.e., the ratio of the surface activity coefficients is assumed to equal 1.0 (*42*). Note that the model significantly underpredicts Pb(II) sorption at pH <4.0. Although not evident in the figure, the model also overpredicts Pb(II) sorption at pH >6. The same was true for the $(\equiv FeO)_2Pb/\equiv FeOPb^{+}-NO_3^{-}$ species pair (Figure 4b). The nonzero plateau in the pH edge data at low pH seems questionable at first; however, others have also reported pH edges for divalent metal sorption onto amorphous ferric hydroxides with this same phenomenon (*4, 46−50*). In addition, extensive isotherm and edge data for trace metal sorption onto ferrihydrite are being collected in our lab at low pH. Preliminary results to be reported in a future paper indicate that there is nonzero sorption at pH <4.0. The sorption plateau at low pH seems to be most prominent for ferrihydrite at low metal-to-sorbent ratios (i.e., in dilute systems). For example, note the difference in the pH edges for sorption of 800 μM Pb(II) onto 1.0 g versus 0.1 g of ferrihydrite/L (Figure S9, Supporting Information). The plateau is absent at 0.1 g of ferrihydrite/L. Interestingly, Dzombak and Morel (*1*) report essentially no pH edge data for divalent metals below pH 4.0−4.5. Sorption at pH less than 4.0 has not been extensively studied.

Figure 4a also shows that model curves for the $(\equiv FeO)_2Pb/\equiv FeOHPb^{2+}$ species pair display a much stronger ionic strength dependence than suggested by the 0.1 M $NaNO_3$ data. This is an artifact of the modified TLM thermodynamic framework itself. First, bulk solution concentrations and activity coefficients for the sorbing ions (i.e., H^+, NO_3^-, Na^+, and Pb^{2+}) are used in the mass law expressions (because we know how to measure and estimate them, respectively) rather than true surface species activities themselves (*44*). Second, lacking a way to directly determine the activity of a surface complex as well as a predictive model for estimating surface activity coefficients, the ratio of the activity coefficients for the surface species [i.e., $(\equiv FeO)_2Pb$, $\equiv FeOHPb^{2+}$, and $\equiv FeOH$] is assumed to equal 1.0. In essence, this represents only a "partial correction" for nonidealities at the surface. To correct

for the overprediction of the ionic strength dependence, a surface activity term (γ_s) was used in the OLI model to better match the pH edge data. Interestingly, the best agreement between the predicted curves and the actual data was obtained when γ_s was set equal to γ_{Pb2^+}, the bulk solution activity coefficient for the Pb^{2+} ion. The γ_s term was also used during regression of the isotherm data for the $(\equiv FeO)_2Pb/\equiv FeOHPb^{2+}$ species pair; therefore, the equilibrium constants given in Table 2 include this correction.

Interestingly, ionic strength dependence is less with the species pair, $(\equiv FeO)_2Pb/\equiv FeOPb^+-NO_3^-$, as shown in Figure 4b. Criscenti and Sverjensky (*51*) found that surface species of the form $\equiv FeOPb^+-NO_3^-$, $\equiv FeOHPb^{2+}-NO_3^-$, etc. better represented the ionic strength dependence of metal sorption in nitrate solutions. At the present time, spectroscopy is unable to confirm whether this type of surface species actually exists at the surface or whether it is necessary because of the construct of the TLM thermodynamic framework itself.

Figure 4c,d displays TLM predictions for both species pairs when pH-adjusted *K* values are used rather than the best-fit equilibrium constants for pH 4.5−5.5 only. In other words, log *K* values for the Pb surface complexes in the model were adjusted with pH as reported in Table 2. In addition, Figure 4c includes the γ_s correction. Note the good agreement between the model curves and the actual data. The better fit at pH <4 was accomplished without introducing a second, high-affinity site type or additional surface species as has often been done in past modeling studies that are based on pH edge data only. Although not shown, introducing a second, high-affinity site to account for the elevated Pb(II) sorption at pH <4 resulted in unacceptable fits of the isotherm data at low Pb(II) concentrations. Instead, when considered together, the isotherm and edge data suggest that a one-site, two-species model is sufficient but that the best-fit equilibrium constants are valid over a limited pH range only. Additional pH edge data from ref *26* at different Pb(II):Fe ratios were also compared against the TLM-predicted edges (Figures S9 and S10, Supporting Information).

Implications for Surface Complexation Modeling. This study highlights the benefits of combining comprehensive molecular- and macroscopic-scale studies conducted by the same researcher in the same laboratory with surface complexation modeling. Regressing constant-pH isotherm data together with potentiometric titration and pH edge data is clearly a much more rigorous test of the SCM. When combined with spectroscopic data on surface speciation, the scope of feasible surface complexes and site types becomes much more limited. In this work, application of the triple-layer SCM led to the same conclusions about Pb(II) speciation on the ferrihydrite surface as did analysis of the spectroscopic data in ref *26*. More specifically, the authors found that regressing pH edge data in the absence of isotherm and spectroscopic data resulted in a much larger number of surface-species and site-type combinations that provided acceptable fits of the edge data. However, when these same assumptions were used to predict the constant-pH isotherms, the agreement between model and data was poor in most cases. Finally, the results of this research suggest that a single set of SCM thermodynamic parameters is unable to predict single-solute Pb(II) sorption onto ferrihydrite over a wide range of conditions. While many advances have been made over the past decade, much more work still needs to be done in fine-tuning the thermodynamic framework and databases.

Acknowledgments

This research was supported by funding from the DuPont Company and the State of Delaware through the Delaware Research Partnership. The authors particularly thank Drs. Jehangir Vevai and Hugh Campbell for their financial support and Mr. Steve Sanders and Dr. Marshall Rafal, OLI Systems, Inc., for their important contributions to the implementation of surface complexation models in the OLI Software. We are also grateful to three anonymous reviewers for their comments.

Supporting Information Available

Two graphs showing NEM and GTLM fits of potentiometric titration data; graph showing triplicate sets of 0.1 M $NaNO_3$ potentiometric titration data; three graphs showing TLM fits of constant-pH isotherm data using a one-species model; one graph showing TLM isotherm fits using the species pair, $\equiv FeOPbOH/\equiv FeOPb^+$; two graphs showing GTLM fits of isotherm data; two graphs showing TLM fits of additional pH-sorption-edge data using the species pairs, $(\equiv FeO)_2Pb/\equiv FeOHPb^{2+}$ and $(\equiv FeO)_2Pb/\equiv FeOPb^+-NO_3^-$; table of equilibrium reactions and associated equilibrium constants used in OLI code; OLI activity coefficient model. This material is available free of charge via the Internet at http://pubs.acs.org.

Nomenclature

a_i	activity of species *i*
A_s	specific surface area of sorbent (m^2/g)
C_A	quantity of mineral acid added during potentiometric titration of sorbent (equiv/L)
C_B	quantity of mineral base added during potentiometric titration of sorbent (equiv/L)
C_1	inner-layer capacitance term for triple-layer model (faraday/m^2)
C_2	outer-layer capacitance term for triple-layer model (faraday/m^2)
F	Faraday's constant (96 485 C/mol)
$[H^+]$	hydrogen ion molal concentration (mol/kg of H_2O)
K_i	conditional equilibrium constant
K_i^{int}	intrinsic or thermodynamic equilibrium constant
K_{a1}^{int}	intrinsic acidity constant for the surface deprotonation reaction: $\equiv FeOH_2^+ = \equiv FeOH + H^+$
K_{a2}^{int}	intrinsic acidity constant for the surface deprotonation reaction: $\equiv FeOH = \equiv FeO^- + H^+$
N_s	surface site density (mol of sites/mol of sorbent)
$[OH^-]$	hydroxyl ion molal concentration (mol/kg of H_2O)
q	excess acid added during potentiometric titration (equiv/L)
R	gas constant (8.314 J K^{-1} mol^{-1})
R_{avg}	arithmetic average of nonlinear regression fit parameters obtained from the OLI Software (R_i for each data point is the ratio of the model-calculated value to the experimental value (or vice versa), such that R_i is 1.0 or higher)
T	absolute temperature (K)
ΔpK_a	equals ($pK_{a2}^{int} - pK_{a1}^{int}$) when the protonation/deprotonation reactions are written as dissociation reactions
γ_s	lumped surface activity coefficient used in OLI model to account for nonidealities of the surface complex species
Γ	surface loading (mol of Pb(II)/mol of Fe)

Ψ_o electric potential at o-plane in TLM or at surface in GTLM

Ψ_β electric potential at β-plane in TLM

Literature Cited

(1) Dzombak, D. A.; Morel, F. M. M. *Surface Complexation Modeling: Hydrous Ferric Oxide*; John Wiley & Sons: New York, 1990.
(2) Scheinost, A. C.; Abend, S.; Pandya, K. I.; Sparks, D. L. *Environ. Sci. Technol.* **2001**, *35*, 1090−1096.
(3) Benjamin, M. M. Effects of Competing Metals and Complexing Ligands on Trace Metal Adsorption at the Oxide/Solution Interface. Ph.D. Dissertation, Stanford University, Stanford, CA, 1979.
(4) Davis, J. A.; Leckie, J. O. *J. Colloid Interface Sci.* **1978**, *67*, 90−107.
(5) Balistrieri, L. S.; Murray, J. W. *Geochim. Cosmochim. Acta* **1982**, *46*, 1253−1265.
(6) Catts, J. G.; Langmuir, D. *Appl. Geochem.* **1986**, *1*, 255−264.
(7) Hunter, K. A.; Hawke, D. J.; Choo, L. K. *Geochim. Cosmochim. Acta* **1988**, *52*, 627−636.
(8) Cowan, C. E.; Zachara, J. M.; Resch, C. T. *Environ. Sci. Technol.* **1991**, *25*, 437−446.
(9) Kanungo, S. B. *J. Colloid Interface Sci.* **1994**, *162*, 93−102.
(10) Gunneriusson, L.; Lovgren, L.; Sjoberg, S. *Geochim. Cosmochim. Acta* **1994**, *58*, 4973−4983.
(11) Kooner, Z. S.; Cox, C. D.; Smoot, J. L. *Environ. Toxicol. Chem.* **1995**, *14*, 2077−2083.
(12) Christl, I.; Kretzschmar, R. *Geochim. Cosmochim. Acta* **1999**, *63*, 2929−2938.
(13) Katz, L. E.; Hayes, K. F. *J. Colloid Interface Sci.* **1995**, *170*, 477−490.
(14) Katz, L. E.; Hayes, K. F. *J. Colloid Interface Sci.* **1995**, *170*, 491−501.
(15) Robertson, A. P.; Leckie, J. O. *Environ. Sci. Technol.* **1998**, *32*, 2519−2530.
(16) Hayes, K. F. Equilibrium, Spectroscopic, and Kinetic Studies of Ion Adsorption at the Oxide/Aqueous Interface. Ph.D. Dissertation, Stanford University, Stanford, CA, 1987.
(17) Brown, G. E., Jr.; Parks, G. A.; Bargar, J. R.; Towle, S. N. In *Mineral−Water Interfacial Reactions: Kinetics and Mechanisms*; Sparks, D. L., Grundl, T. J., Eds.; ACS Symposium Series 715; American Chemical Society: Washington, DC, 1998; pp 14−36.
(18) Katz, L. E.; Boyle-Wight, E. J. In *Physical and Chemical Processes of Water and Solute Transport/Retention in Soil*; Selim, H. M., Sparks, D. L., Eds.; SSSA Special Publication 56; Soil Science Society of America: Madison, WI, 2001; pp 213−255.
(19) Koretsky, C. *J. Hydrol.* **2000**, *230*, 127−171.
(20) Sverjensky, D. A.; Sahai, N. *Geochim. Cosmochim. Acta* **1996**, *60*, 3773−3797.
(21) Sahai, N.; Sverjensky, D. A. *Geochim. Cosmochim. Acta* **1997**, *61*, 2827−2848.
(22) Koretsky, C. M.; Sverjensky, D. A.; Sahai, N. *Am. J. Sci.* **1998**, *298*, 349−438.
(23) Sverjensky, D. A. *Geochim. Cosmochim. Acta* **2001**, *65*, 3643−3655.
(24) Kulik, D. A. *Geochim. Cosmochim. Acta* **2000**, *64*, 3161−3179.
(25) Kulik, D. A. *Am. J. Sci.* **2002**, *302*, 227−279.
(26) Trivedi, P.; Dyer, J. A.; Sparks, D. L. *Environ. Sci. Technol.* **2003**, *37*, 908−914.
(27) Dyer, J. A. Advanced Approaches for Modeling Trace Metal Sorption in Aqueous Systems. Ph.D. Dissertation, University of Delaware, Newark, DE, 2002.
(28) Sanders, S. J.; Rafal, M.; Clark, D. M.; Young, R. D.; Scrivner, N. C.; Pease, R. A.; Grise, S. L.; Diemer, R. B. *Chem. Eng. Prog.* **1988**, *92*, 47−54.
(29) Rafal, M.; Black, P.; Sanders, S. J.; Tolmach, P. I.; Young, R. D. *Development of a Comprehensive Environmental Simulation Program*; Presented at the AIChE Spring National Meeting, Atlanta, GA, April 17−21, 1994.
(30) Glushko, V. P.; Medvedev, V. A.; Bergman, G. A.; Vasil'ev, B. P.; Kolesov, W. P.; Gurvich, L. V.; Yungmand, V. S.; Khodakovskii, I. L.; Resnitskii, L. A.; Smirnova, N. L.; Gal'chenko, G. L.; Alekseev, V. I.; Vorob'ev, A. F.; Baibuz, V. F.; Kostryukov, B. N.; Biryokov, B. P. *Thermo Constants of Compounds*, Vols. 1−10; Academy of Sciences: Moscow, USSR, 1965−1981.
(31) Wagman, D. D.; Evans, W. H.; Parker, V. B.; Schumm, R. H.; Halow, I.; Bailey, S. M.; Churney, K. L.; Nuttall, R. L. *J. Phys. Chem. Ref. Data* **1982**, *11*, 1−392.
(32) Gurvich, L. V.; Veyts, I. V.; Medvedev, V. A.; Khachkuruzov, G. A.; Yungman, V. S.; Bergman, G. A.; Iorish, V. S.; Yurkov, G. N.; Gorbov, S. I.; Kuratova, L. F.; Trishcheva, N. P.; Przheval'skiy, I. N.; Leonidov, V. Ya.; Ezhov, Yu. S.; Tomberg, S. E.; Nazarenko, I. I.; Rogatskiy, A. L.; Dorofeyeva, O. V.; Demidova, M. S. *Thermodynamic Properties of Individual Substances*, 4th ed., Vols. 1−5; USSR Academy of Sciences, Institute for High Temperatures and State Institute of Applied Chemistry; Hemisphere Publishing Corp.: New York, 1989.
(33) Chase, M. W., Jr.; Davies, C. A.; Downey, J. R., Jr.; Frurip, D. J.; McDonald, R. A.; Syverud, A. N. *J. Phys. Chem. Ref. Data* **1985**, *14* (Suppl. 1), 1−1856.
(34) Daubert, T. E.; Danner R. P. *Physical and Thermodynamic Properties of Pure Chemicals*: *DIPPR Data Compilation*; Hemisphere Publishing Corp.: New York, 1989.
(35) Oelkers, E. H.; Helgeson, H. C.; Shock, E. L.; Sverjensky, D. A.; Johnson, J. W.; Pokrovskii, V. A. *J. Phys. Chem. Ref. Data* **1995**, *24*, 1401−1560.
(36) Rafal, M.; Berthold, J. W.; Scrivner, N. C.; Grise, S. L. In *Models for Thermodynamic and Phase Equilibria Calculations*; Sandler, S. I., Ed.; Marcel Dekker: New York, 1994; pp 601−670.
(37) Zemaitis, J. F., Jr.; Clark, D. M.; Rafal, M.; Scrivner, N. C. *Handbook of Aqueous Electrolyte Thermodynamics: Theory and Application*; Design Institute for Physical Property Data, American Institute of Chemical Engineers, Inc.: New York, 1986.
(38) Shock, E. L.; Helgeson, H. C. *Geochim. Cosmochim. Acta* **1988**, *52*, 2009−2036.
(39) Anderko, A.; Sanders, S. J.; Young, R. D. *Corrosion* **1997**, *53*, 43−53.
(40) Scrivner, N. C.; Butler, P. B.; Karmazyn, J. *Modeling: An Excellent Solution for Remediation*; Presented at the 69th Annual Conference and Exposition of the Water Environment Federation, Session 5, Dallas, TX, October 5−9, 1996.
(41) Hayes, K. F.; Katz, L. E. In *Physics and Chemistry of Mineral Surfaces*; Brady, P. V., Ed.; CRC Press: Boca Raton, FL, 1996; pp 147−223.
(42) Sahai, N.; Sverjensky, D. A. *Comput. Geosci.* **1998**, *24*, 853−873.
(43) Sparks, D. L. *Environmental Soil Chemistry*; Academic Press: San Diego, CA, 1995.
(44) Robertson, A. P.; Leckie, J. O. *J. Colloid Interface Sci.* **1997**, *188*, 444−472.
(45) Hsi, C.-K. D.; Langmuir, D. *Geochim. Cosmochim. Acta* **1985**, *49*, 1931−1941.
(46) Swallow, K. C.; Hume, D. N.; Morel, F. M. M. *Environ. Sci. Technol.* **1980**, *14*, 1326−1331.
(47) Benjamin, M. M.; Bloom, N. S. In *Adsorption from Aqueous Solutions*; Tewari, P. H., Ed.; Plenum Press: New York, 1981; pp 41−60.
(48) Benjamin, M. M. *Environ. Sci. Technol.* **1983**, *17*, 686−692.
(49) Harvey, D. T.; Linton, R. W. *Colloids Surf.* **1984**, *11*, 81−96.
(50) Misak, N. Z.; Ghoneimy, H. F.; Morcos, T. N. *J. Colloid Interface Sci.* **1996**, *184*, 31−43.
(51) Criscenti, L. J.; Sverjensky, D. A. *Am. J. Sci.* **1999**, *299*, 828−899.

Received for review May 16, 2002. Revised manuscript received December 6, 2002. Accepted December 13, 2002.

ES025794R